Technical Memo

ECMWF
European Centre for Medium-Range Weather Forecasts

932

Sea-ice concentration analysis in model space in IFS cycle CY49R1

S. Massart and A. J.Geer

September 2025

Series: ECMWF Technical Memoranda

A full list of ECMWF Publications can be found on our web site under:
http://www.ecmwf.int/en/publications/

Contact: library@ecmwf.int

Abstract

Recent developments, implemented in operations in November 2024, allowed surface-sensitive microwave observations to be assimilated over sea ice in the atmospheric 4D-Var of the European Centre for Medium-range Weather Forecasts (ECMWF). Those developments were based on the framework of the observation-space auxiliary control variables (TOVSCV) that extends the control vector with observation-space variables at observation locations. They provide an estimation of both the sea ice concentration (SIC) and some additional empirical variables that describe the physical state of the sea ice.

In this paper, we describe an alternative framework that extends the Integrated Forecasting System (IFS) control vector with a model-space variable that represents the sea ice concentration. We compare the two approaches over two periods of 3 months each, one in Boreal and one in Austral summer, while using the sea ice sensitive radiances for the Advanced Microwave Scanning Radiometer 2 (AMSR2) and the GPM Microwave Imager (GMI).

The two approaches provide an analysis with similar values for the sea ice concentration, with differences between 2-3% in mean value. One important difference between the two approaches is the method used to compute background values of sea ice concentration used for cycling the assimilation system. In the observation-space framework, the background values are derived from the dynamically retrieved surface emissivity in the 10 GHz channel for each observation. In the model-space framework, the analysis sea ice field from the previous analysis update is used as the background. Using this approach, the first-guess departure for the both AMSR2 and GMI is generally less biased, but presents a larger standard deviation. Despite this, the forecast scores are neutral to sightly positive for the model-space approach compared to the observation-space one.

Plain Language Summary

Numerical weather prediction (NWP) systems use data from ground-based platforms, satellites, and computer models to create the most accurate starting point for forecasting the weather for the next few days. Satellite data, especially radiances, play a key role by providing important information about the atmosphere, such as temperature and humidity, and also about the Earth's surface. Specifically, most NWP systems use some indirect data from on-board microwave sensors that have strong sensitivity to the surface over sea ice, which is the focus of this document.

From November 2024, the European Centre for Medium-Range Weather Forecasts (ECMWF) started to directly use observations from microwave sensors with strong sensitivity to the sea ice in making atmospheric forecasts in its Integrated Forecasting System (IFS). This was possible thanks to an approach that provides sea ice information, but only at the location of the observations.

In this document, we review this approach and show how it can be used to generate full maps of sea ice concentration. We compare it to the previous method and find that both give similar results for sea ice concentration and forecast accuracy. However, the updated approach has advantages that could support future developments.

1 Introduction

Data assimilation systems in numerical weather prediction (NWP) aim to produce the most accurate initial conditions for Earth system forecasting. This is achieved by integrating data from ground-based platforms, satellite instruments, and numerical forecast models. The combination of these various data sources results in what is known as the analysis (Le Dimet and Talagrand, 1986). Satellite radiances play a significant role in improving the quality of the analysis by providing essential information about the atmospheric state, such as temperature and humidity (Bormann *et al.*, 2019). Additionally, they offer insights into other components of the Earth system, particularly the condition of the Earth's surface. In this document, we focus specifically on microwave radiances from channels sensitive to sea ice concentration (SIC), a significant surface variable in polar regions.

Atmospheric data assimilation systems typically do not directly include sea ice concentration. Yet, they often require information on sea ice. At the European Centre for Medium-range Weather Forecasts (ECMWF), in the current operational version (cycle CY49R1), the sea ice analysis is part of a separate ocean data assimilation system (OCEAN5, Zuo *et al.*, 2019). The sea ice concentration initial condition is derived from the preceding analysis of the OCEAN5 operational assimilation system and passed to the next 4D-Var atmospheric analysis. Within the data assimilation window, the sea ice concentration does not evolve and remains constant.

The OCEAN5 system assimilates third-party SIC retrievals. This has significant practical and scientific problems for the atmospheric analysis as detailed in Geer (2024a). Mainly, there could be a delay from 48 hours up to 72 hours for the SIC information compared to the validity time of the observations used to generate it, due to a complex processing chain from the retrievals to the atmospheric analysis. Moreover, it is sub-optimal to use the same satellite observation directly in the atmospheric analysis and indirectly in a third-party surface state retrieval. A cleaner way to make optimal use of the observations is to jointly estimate the atmospheric and surface states from the radiances. This idea led to the sea ice developments of Geer (2024a) that have been implemented in November 2024 as part of cycle CY49R1 of the ECMWF Integrated Forecasting System (IFS).

Previously to the work of Geer (2024a), surface-sensitive radiances have not been used over sea ice at ECMWF because of the need to link the surface state to the observed radiance through a radiative transfer model. The first problem was that many of the state variables that affect the radiative transfer were not well known. The second problem was that there was also a relative lack of accuracy of current models for radiative transfer in the surface sea ice. A solution was proposed by combining machine learning and data assimilation to simultaneously learn from the observations both the unknown physical state of the surface and the forward model for the radiative transfer (Geer, 2024b). This allowed surface-sensitive microwave observations to be assimilated over sea ice in the atmospheric 4D-Var, estimating both the SIC and some additional empirical variables that describe the physical state of the sea ice.

The Geer (2024a) implementation was based on the framework of the observation-space auxiliary control variables that consists in extending the control vector with observation-space variables at observation locations. This has been used for several decades at ECMWF as a sink variable for radiance observations (Eyre *et al.*, 1992). Recently Massart *et al.* (2021) investigated the benefits of moving the observation-space skin temperature (SKT) analysis to a model-space one. In a nutshell, the control vector was extended with a two-dimensional XSKT field and each observation that would require SKT would interpolate this XSKT field at the observation location.

In this document, we investigate the benefits of moving the observation-space SIC analysis of Geer (2024a) to a model-space one as done for SKT. The next section details the differences between the two approaches and their settings. The following section presents and discuss some results from the two approaches, before concluding in the last section.

2 Method

2.1 Overview

The new developments are tested within the atmospheric data assimilation system, built upon a baseline (or Control) that represents the IFS cycle CY49R1 used by Geer (2024a). This baseline configuration uses a resolution of O400 (about 25 km horizontally). The atmospheric data assimilation system employs a non-overlapping 12-hour window 4D-Var, and an incremental method with three inner loops. The last inner loop uses a resolution of N128 (about 80 km). Deterministic 10-day forecasts are generated twice daily from the 4D-Var windows, with start times at 0000 and 1200 UTC.

The control and model-space sea ice analysis configurations are compared over two 3-month long experiments in each configuration: one starting from 1st June 2022 and running until the end of August 2022 (Boreal summer referred to as JJA hereafter) and another starting 1st December and running until the end of February 2023 (Austral summer referred to as DJF hereafter). The initial 5 days are discarded as spin-up.

2.2 Sea ice assimilation framework

Geer (2024a) applied the sea ice assimilation framework to two of the microwave imagers: the Advanced Microwave Scanning Radiometer 2 (AMSR2) and the GPM Microwave Imager (GMI), with a selection of specific channels for sea ice detailed in Tab 1. They augmented the 4D-Var control vector with four observation-space variables: the sea ice concentration and three sea ice empirical states. Their observation-space variables were activated for each AMSR2 and GMI scene where the sea surface temperature was lower than 277 K and the land fraction lower than 0.01.

Table 1: Channel usage over oceans in the sea ice assimilation configuration: x, unused or passive in the data assimilation; A, active for atmospheric data assimilation; S, active for sea ice and atmospheric data assimilation; -, channel does not exist. Table extracted from Geer (2024a)

Channel	AMSR2 ocean	AMSR2 sea ice	GMI ocean	GMI sea ice
10v	x	S	x	S
10h	x	S	x	S
19v	A	S	A	S
19h	A	S	A	S
24v	A	S	A	S
24h	A	S	-	-
37v	A	S	A	S
37h	x	x	x	x
89v	A	S	A	S
89h	x	x	x	x
166v	-	-	A	x
166h	-	-	A	x
183±7v	-	-	A	x
183±3v	-	-	A	A

In contrast to Geer (2024a), our sea ice concentration analysis takes place in model-space. We introduce a two-dimensional sea ice concentration field to the control vector, following the approach of Massart *et al.* (2021). This new field is referred to as XSIC (eXtended control vector - Sea Ice Concentration). For each GMI and AMSR2 observation, when required, the sea ice concentration used in the observation operators is derived from the same XSIC field, interpolated at the observation location. To mimic the setting of Geer (2024a), we allow an XSIC increment only where the sea surface temperature is lower than 277 K and the land fraction lower than 0.01.

The XSIC field does not have a model for its propagation within the assimilation window. Instead, it is valid for the whole assimilation window. This adds a strong constraint compared to the observation-space approach. The time-variability of the sea ice concentration within 12-hours can not be represented. We tried to have hourly XSIC fields as in Massart *et al.* (2021), but we found unrealistic time-variability due to the difference between GMI and AMSR2 in the local time of the overpasses. Therefore, we discarded this option.

For the three sea ice empirical states, we have the option of using the observation-space framework as in Geer (2024a) or the model-space framework. In this document, we present only the first option, focussing

on the sea ice concentration. The three sea ice empirical states will be referred to as EP1, EP2 and EP3 respectively.

2.3 Assimilation setting

The background value for the sea ice concentration control variable in observation-space is taken from a sea ice concentration retrieval rather than the available sea ice estimate from OCEAN5 (Geer, 2024a). The retrieval is based on the dynamically retrieved surface emissivity in the 10 GHz channel for each observation. The retrieval can not be directly used in model-space. Instead, we decided to use the analysed XSIC field from the previous assimilation window as a background. The 12 h time-shift means that we will have some sea ice position errors in our background. This could result in observations being rejected because of the resulting large background departures. On the other hand, we believe the background to be better than the OCEAN5 sea ice estimate which is between around 48 and 72 hours behind instantaneous observations (Geer, 2024b).

Because of the difference in the background between the two approaches, we changed the SIC background error standard deviation compared to Geer (2024a), where it is 0.25. In the model-space approach, 0.125 is used instead. In preliminary experiments where we had the same value, the SIC variable seemed to be used to compensate other errors. The SIC analysis was significantly different between the two approaches as well as the brightness temperature analysis for the various channels of GMI and AMRS2. With the new value of the standard deviation for the model-space approach, the analyses are now similar (see sec. 3). The empirical states EP1, EP2 and EP3 also need to be assigned background errors in the observation-space TOVSCV auxiliary control variable, and for this we kept the same values as the earlier study, i.e. 0.34, 0.34 and 0.3 respectively. The background state for these empirical variables is zero, since it is not easy to cycle the analysed values from one analysis time to the next, given they are not in model space.

For the model-space approach, we have to define the background error correlation structures. We assume them to be relatively small scale, and smaller scale than the resolution of the last inner loop (about 40 km in this study). This implies that the background error correlation would need to be diagonal in gridpoint space. The background error correlation for the XSIC field is implemented following the wavelet approach (Fisher and Andersson, 2001). This means that it is not possible to have a strictly diagonal matrix in gridpoint space. Still, we set the wavelet coefficient to be as close as possible to a diagonal matrix. As a first step, we assume that the sea ice background error is not correlated with other variables of the control vector.

The atmospheric data assimilation system is a 12-hour window incremental 4D-Var with several outer loop updates. Each update has an iterative procedure of minimizing the incremental control variable (inner loop) at lower resolution than the outer loop. In the observation-space approach, the analysis of XSIC and of the empirical states at the end of each inner loop is directly used as a first guess for the next inner loop.

In the model-space framework, the two-dimensional increments obtained after each inner loop are extrapolated at the outer loop resolution using a bi-conservative interpolation. This means that even with a diagonal background error correlation matrix, in case of an isolated iceberg, we may be able to detect it, but the accuracy of its location will depend on the resolution of the last inner loop (N128 in this memo). On the other hand, the GMI and AMSR2 observations are superobbed on a N256 grid, which also limits the detection of the iceberg location to this resolution.

In the operational forecast system, the resolution of the last inner loop is currently N400. The limiting factor would thus be the superobbing resolution. The relationship between the last inner loop resolution and the superobbing resolution may make the results described here not entirely reproducible at higher resolutions. In this work, for the last inner loop of N128 resolution, we may have up to 4 observations per

grid cell per satellite overpass, with up to 7 overpasses a day for AMSR2. In the model-space approach, all these points are assigned the same SIC value, whereas they would have their own individual value in the observation-space approach.

We did some preliminary tests with changing the superobbing on a N128 resolution grid to match the resolution of the last inner loop. The comparison of the two approaches using this superobbing resolution provided similar conclusions to the ones of this memo. We thus decided to keep the original superobbing resolution, allowing us to use as a control the standard experiment that serves as a reference for the IFS cycle we are using (CY49R1).

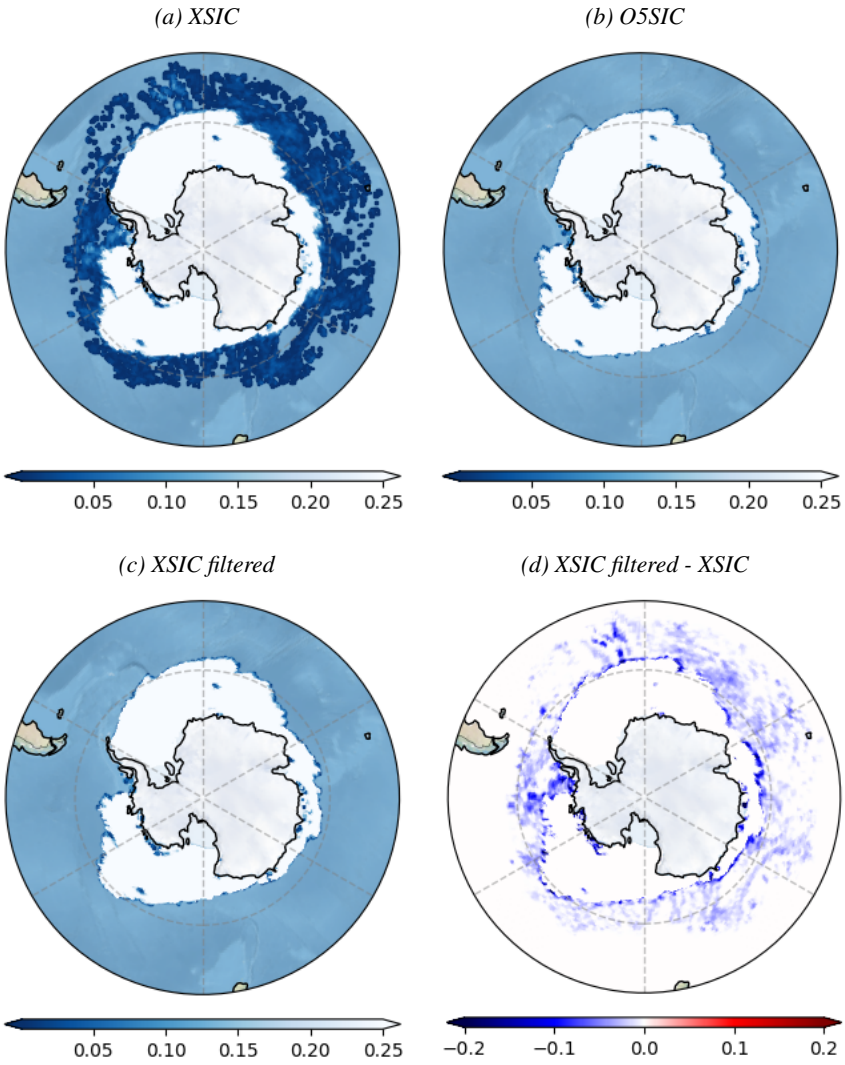

Figure 1: Example of the XSIC analysis filtering: (a) XSIC analysis on 1st December 2022, (b) OCEAN5 sea ice, (c) filtered XSIC analysis used as the background for the next cycle and (d) difference between (a) and (c). Note that non-zero SICs are overlaid on an ocean background in panels (a-c), which is also shown in mid-blue hues, but this does not indicate any sea ice concentration.

2.4 Analysis filtering

Unrepresented supercooled liquid cloud and rain in the IFS model is suspected to produce spurious ice in the sea ice analysis. Similarly to Geer (2024a), we filter the SIC values lower than 0.25 in the analysis.

This is required in this context because the analysis is used as a background for the next assimilation cycle.

Our filter relies on the values of empirical state and sea ice concentration. The process begins by interpolating the analysed values of these variables onto the N256 thinning grid for each observation. If only a single overpass from one instrument were available, each variable would have at most one value per grid point on the target grid. However, since we assimilate two instruments and multiple overpasses, we aggregate the values from all overpasses and instruments at each grid point, and then compute the average. We have observed that the empirical states remain near zero in areas that appear to be false sea ice that has been generated to fit the missing liquid water cloud. Hence, if at a given grid point, the absolute value of the averaged empirical states falls below 0.01 and the mean sea ice concentration is less than 0.25, we conclude that sea ice should not be present at that location.

The process allows to build a mask on the N256 grid. The mask is then linearly interpolated at the outer loop resolution. Figure 1 presents the result of such a process.

3 Results

We have two sets of experiments for each of the two seasons: the controls (or **CTR**), and the experiment with SIC in the XCV fields (or **XSIC**). As discussed previously, there are two main differences between the **XSIC** experiment in comparison to the control one: (i) the sea ice concentration analysis is performed in model space rather than observation space, and (ii) the background field is derived from the SIC analysis of the preceding assimilation cycle instead of using data from channel 10v. We first evaluate the SIC analyses between the experiments and controls, and then the analyses of the empirical states. Secondly, we assess the quality of the SIC background. Then, we compare the values of the increment and the first guess departure between the experiments. Finally, we compute and evaluate the forecast scores for the two approaches.

3.1 Sea ice concentration analysis

For each GMI or AMSR2 observation, when the sea ice assimilation framework is active, we obtain values of SIC and of EP1 to EP3 from both approaches. We selected data where the SIC value and the absolute values of the empirical states exceeded 10^{-2} and matched them between the two approaches. Appendix A (page 15) presents scatter plots of these aligned datasets, categorized by region, season, and instrument. Additionally, we computed the differences between the two approaches and calculated their mean and standard deviation, with results also grouped by region, season, and instrument (App. B).

The amount of AMSR2 data used is significantly greater than that of GMI, by a factor of approximately 3 during JJA and around 7 during DJF (see Tab. B.2). This is due to GMI having an inclined orbit that only generates observations to about 70° latitude. The difference in sea ice observations is largest in the Northern Hemisphere, particularly during the Boreal summer, where the factor exceeds 60. Since the XSIC field is utilised for both AMSR2 and GMI, it is likely to be more strongly influenced by AMSR2, especially in JJA.

Figure 2 summarises Tab. B.1, displaying only global statistics. With the exception of AMSR2 during JJA, the SIC analysis is, on average, approximately 2 % lower in the **XSIC** experiment. A more detailed examination of the polar regions shows that, apart from areas with high sea ice concentration (above 0.8), the analysis values in the **XSIC** experiment are indeed generally lower than in the control (Fig. A.1). However, for the highest values of the concentration, they are higher in the **XSIC** experiment during JJA.

We have mapped the SIC analysis from observation space into the N256 thinning grid, taking the average

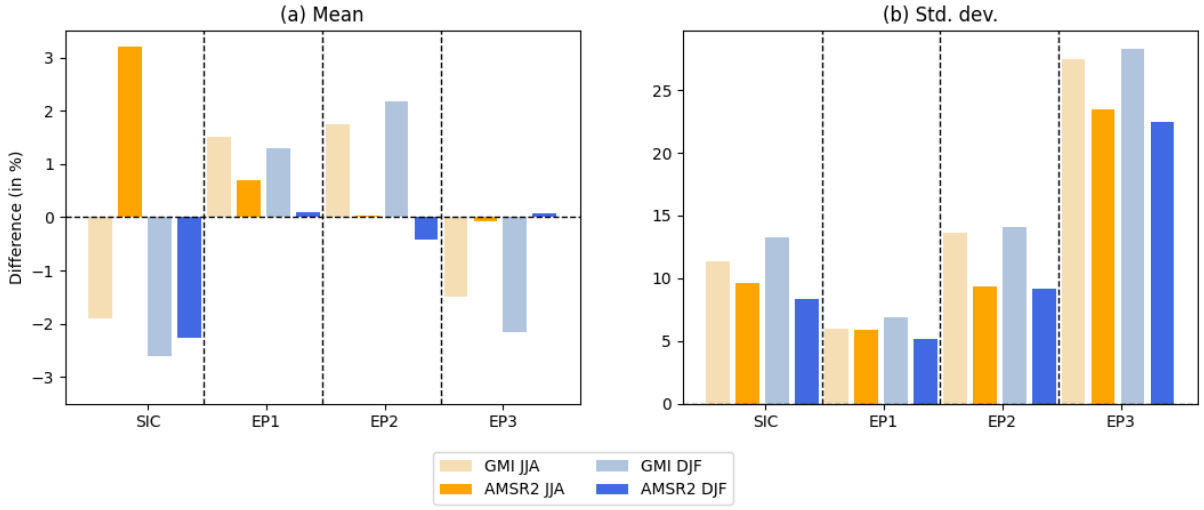

Figure 2: Global mean (a) and standard deviation (b) difference (in %) between the analysed values of the extended variables from model-space and observation-space approaches, computed from all GMI (light colour) or AMSR2 (dark colour) observations using the sea ice framework, when the sea ice concentration analysis is greater than 10^{-2}, for JJA (orange), and DJF (blue): SIC is the sea ice concentration (first set of colour bars), EP1 to EP3 are the empirical states (second to fourth sets of colour bars respectively). The differences are normalised by the background error standard deviation of each variable as used in the control experiment.

of all the data within each grid point. Due to the evolution of the ice pack during the season, the time-average of the mapped field is not meaningful. Instead, we present in App. C a snapshot for the date of 15 July, which is representative of the whole season. In the Northern Hemisphere, the few GMI data are located in the Hudson Bay where the SIC values from the **XSIC** experiment are mainly lower (Figs. C.5a and C.5b). There are many more AMSR2 data available (Figs. C.5c and C.5d). The SIC from this instrument is overall larger in the **XSIC** experiment, except for at the edge of the ice pack. This makes the edges a bit sharper than in the **CTR** experiment. In the Southern Hemisphere, the ice pack edges may also be a bit sharper in the **XSIC** experiment (Figs. C.6b and C.6d). There, the SIC values are still overall larger in the **XSIC** experiment for AMSR2, but they are similar for GMI.

Looking now at the the standard deviation of the difference in the SIC analysis between the two approaches, its value is around 10 % for both instruments and seasons. The values are the highest for GMI during the local summer. The likely explanation is that the analysis is strongly constrained by the respectively numerous AMSR2 observations.

3.2 Empirical states analyses

As for SIC, we have the mean and standard deviation of the difference in analyses of the three empirical states (Fig. 2). Overall, the **XSIC** experiment allows larger (positive and negative) values of the third empirical state than the control. The first two empirical states are most strongly linked to the ice properties, particularly the transition from first year to multi year ice, while the last and third one is not so clearly understood. Hence it might be considered more as an adjustment variable used to fit the emissivity model. The **XSIC** experiment may make more use of this variable to compensate for the difference with the control, namely the fact that we have a single SIC field to interpolate from that is constant for both instruments and for the whole assimilation window. This would explain why for the third empirical state from GMI, the fit between the two approaches is not as good as for the other two (Fig. A.4 versus Figs. A.2 and A.3). This also translates into an increased standard deviation that reaches up to 25 %,

while the values are between 5 % and 15 % for the other states.

3.3 Sea ice concentration increment

We computed the analysis increment (analysis minus background) in observation space, and its spatial average and standard deviation. We expect the mean increment to be small, otherwise this indicates a potential bias in the background. We focus here on AMSR2 as it has more data than GMI, and on JJA.

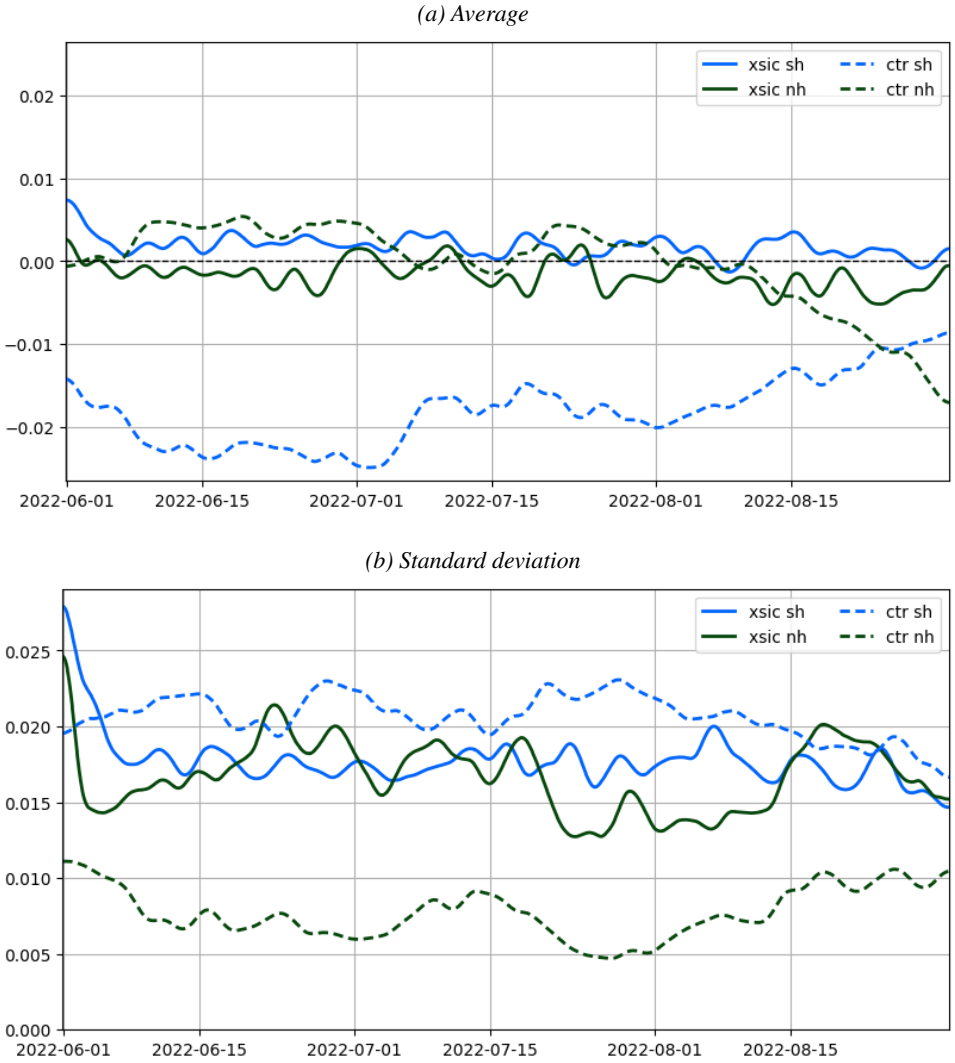

Figure 3: Time series of the SIC (a) mean increment and (b) its standard deviation for the (solid line) **XSIC** *and (dashed line)* **CTR** *experiments, for (blue) Southern and (green) Northern Hemisphere. The curves are smoothed with a 10 day window.*

In the **XSIC** experiment, because the SIC analysis from the previous cycle is used as background, and the ice pack is melting during JJA in the Northern Hemisphere, we expect to have a negative analysis increment. Indeed, a small negative increment is observed (Fig. 3a). In contrast, the **CTR** experiment shows a small positive increment until beginning of August, suggesting that the 10v-derived SIC background may slightly underestimate SIC values.

In the Southern Hemisphere, the opposite effect occurs, with a small positive SIC increment in the **XSIC** experiment and a negative increment in the **CTR** experiment. However, the **CTR** increment is much

larger than the **XSIC** one, indicating that the 10v-derived SIC background may overestimate much the SIC values in this region. In DJF, we have a similar picture but with a swap between the two polar regions: the **CTR** (negative) increment is much larger than the **XSIC** one in the North Polar Region.

The standard deviation of the increment is a measure of the spatial activity of the analysis. For the **XSIC** experiment, it is similar for both hemispheres. For the **CTR** experiment, the standard deviation is relatively low in the Northern hemisphere and relatively large in the Southern Hemisphere. This could indicate that during JJA, on top of a potential bias, the spatial repartition of SIC in the 10v-derived background is less accurate in the Southern Hemisphere than in the Northern hemisphere and than the **XSIC** background.

3.4 First guess departure

The SIC background is used to compute the brightness temperature first guesses for the various channels of GMI and AMSR2. Comparing them with observations gives an indirect measure of the quality of the SIC background. Other variables are used to construct the first guesses, and also contribute to their overall quality. Nevertheless, they do not differ much between the two approaches, and we assume that at the first order, the first guess quality is controlled by the SIC background. Since the background values of the empirical states are set to zero, the interpretation of the difference of the first guess departure between the two experiments is independent from the empirical states.

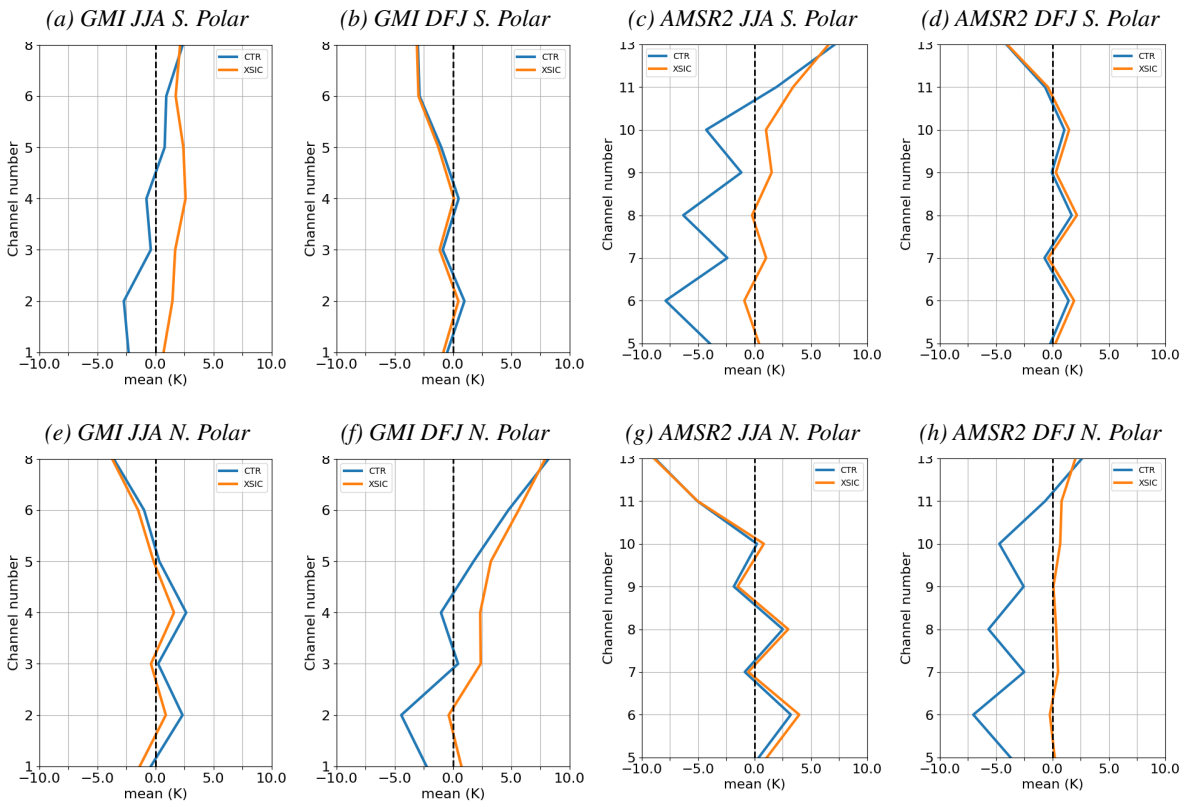

Figure 4: Mean first guess departures (in K*) for GMI (two leftmost pannels) and AMSR2 (two rightmost pannels), Southern (top) and Northen (bottom) Hemisphere and for both seasons (see subcaption). The* **XSIC** *experiment is in orange, while the* **CTR** *one is in blue.*

We focus first on the mean value of the first guess departure (Fig. 4). We discussed previously that on average, the **XSIC** experiment produced SIC values about 3 % higher compared to the control for

AMSR2 in JJA. This translates to an almost unbiased first guess departure for the **XSIC** experiment whereas the **CTR** experiment presents a negative bias of about 5 K in the Southern Polar Region (panel c). In DJF, the difference in SIC values has a similar improvement in mean fit to AMSR2, but over the North Polar Region (panel h). The impact on GMI is more mixed over the South Polar Region and neutral over the North Polar Region (where there are few data points in JJA).

Overall the **CTR** experiment outperformed **XSIC** in terms of first guess departure standard deviation (Fig. 5). The standard deviation was up to twice as much in the **XSIC** experiment. This is expected since the background values are pre-processed in the **CTR** using the 10v channel. This may also result from the pre-processing step which generates a first guess departure with a smoother spatial distribution than that produced by the **XSIC** background.

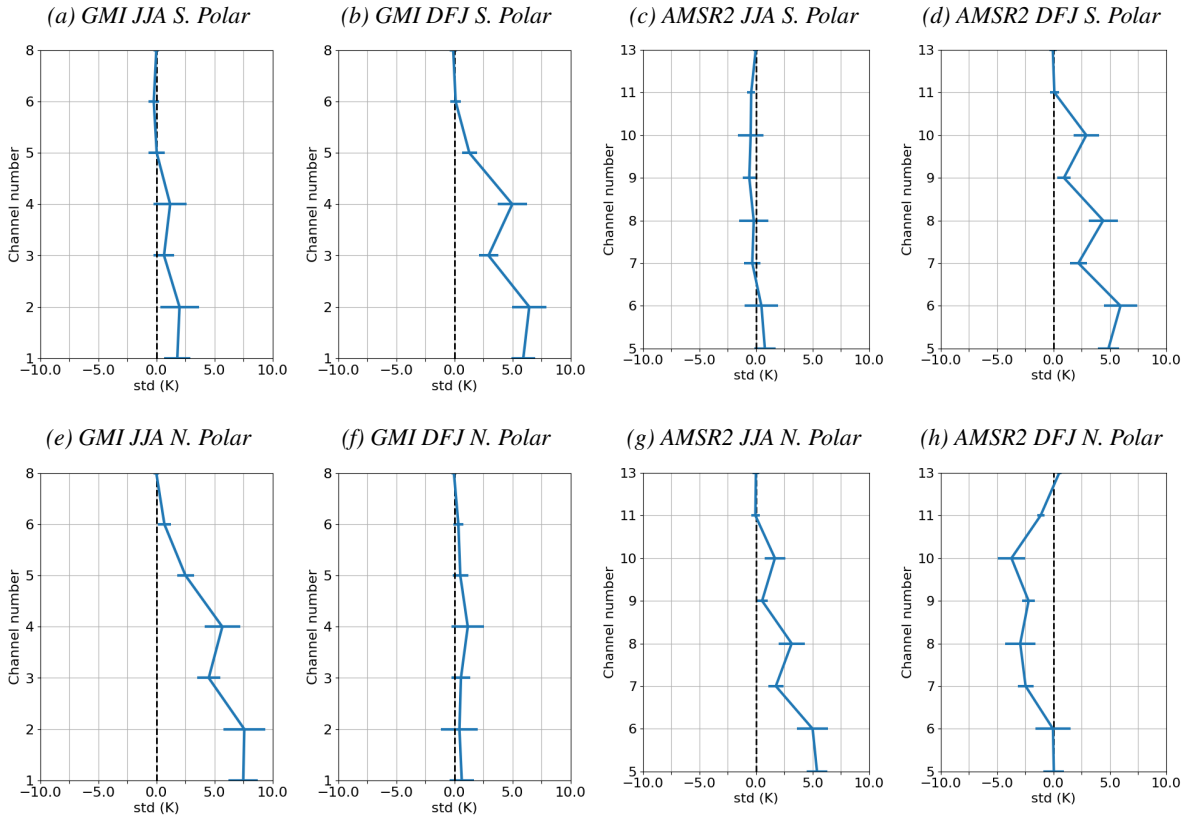

Figure 5: Same as Fig.4 but for the difference in standard deviation of the first guess departure. The error bars indicate a 95% confidence.

In the North Polar Region, for AMSR2 in DJF the **XSIC** experiment outperformed against the control in terms of first guess departure standard deviation (Fig. 5h). The improvement is located mainly in the multi year ice region in the winter, where biases in the AMSR2 SIC observation space retrievals are known to be large (Geer, 2024a). This could hence be a sign of the **XSIC** experiment adapting the background to a climatology that fits the biased AMSR2 SIC retrievals.

3.5 Forecast scores

Overall, the weather parameter forecasts from the **XSIC** experiment are slightly better or comparable to those from the control experiment when evaluated against the operational forecast. As an example, figure 6 shows the temperature differences. The **XSIC** experiment demonstrates a small but statistically significant improvement around the polar ice cap edges in the 12 hour forecast. This improvement

persists for a few days, gradually losing statistical significance. In the medium-range, the differences between the two experiments are not statistically significant enough to clearly identify a superior approach.

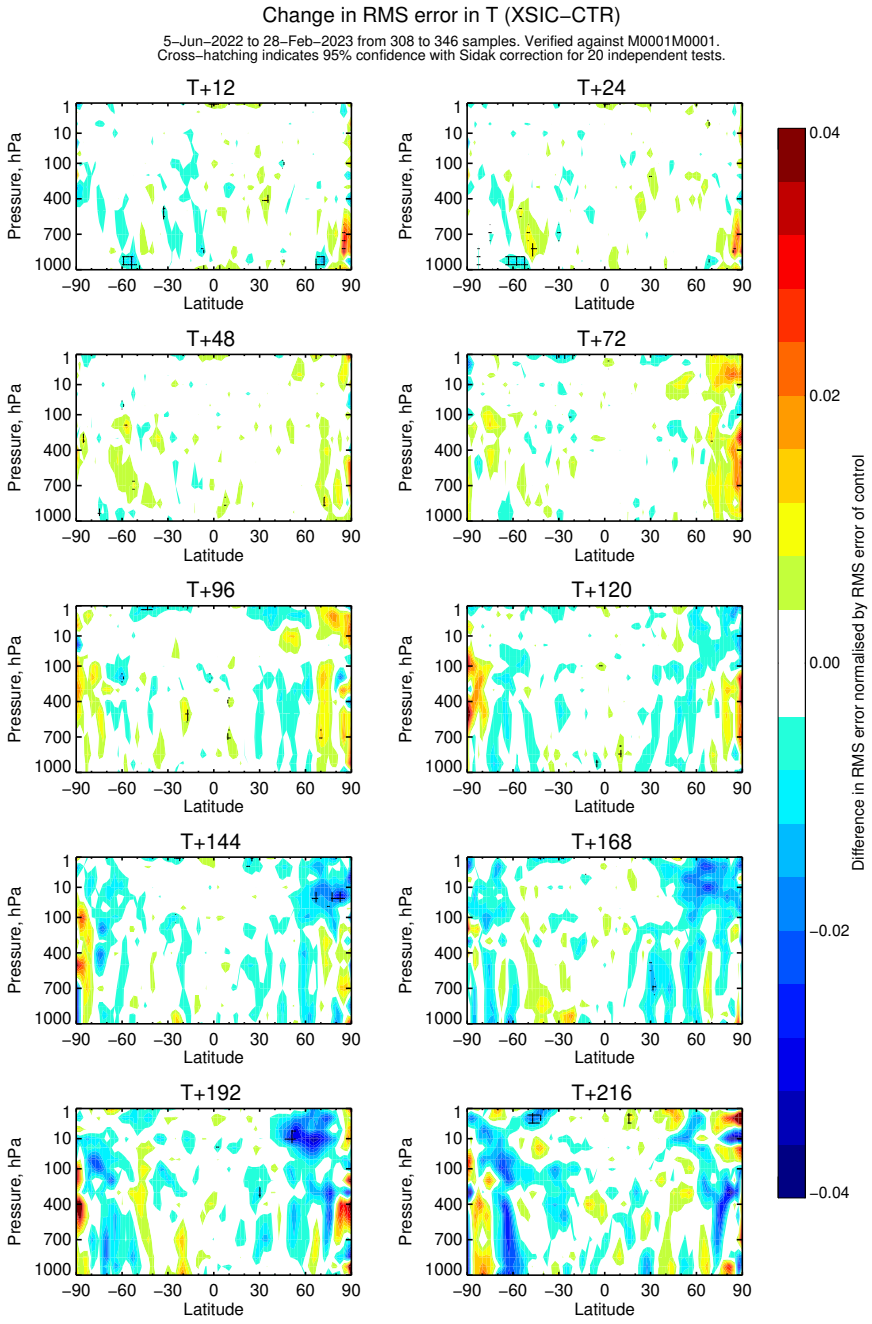

*Figure 6: Zonal mean (latitude vs. model level) of the normalised change in root mean square error in temperature (***XSIC** - **CTR***) for various forecast lead times, compared to the operational forecast. Cross-hatching indicates 95% confidence with Sidak correction for 20 independent tests.*

Comparing the two experiments against observations, we have a statistically significant improvement in the medium-range, for temperature, winds and geopotential (Fig. 7). For example, we have an improvement of the geopotential at 500 hPa at day 5 of more than 2% in the Northern Hemisphere and about 1.5% in the Southern Hemisphere (but, less statistically significant). Those improvements are corroborated when comparing the forecast against the operational analysis, but are not statistically significant.

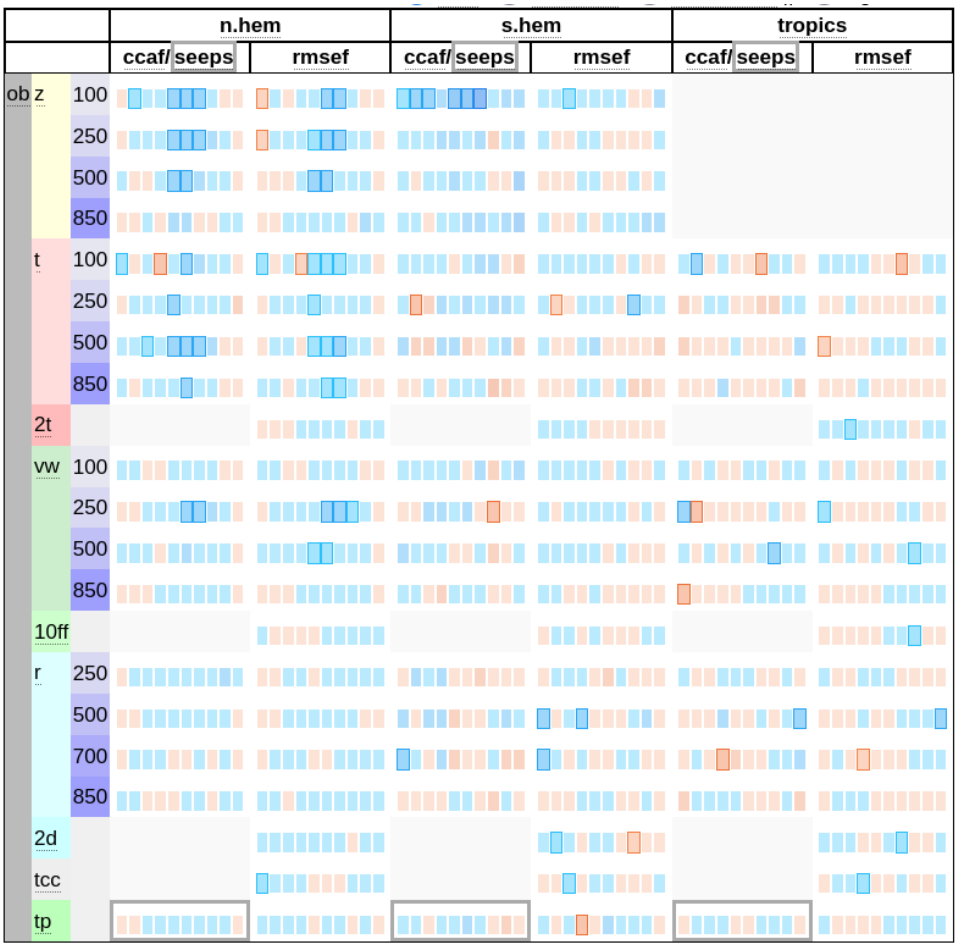

Figure 7: Scorecard of the **XSIC** *experiment versus the* **CTR** *one against observations (model parameters as various pressure levels as a function of forecast lead time). A blue (red) box signifies that the* **XSIC** *experiment outperforms (underperforms) the* **CTR** *experiment, and a dark colour indicates 95% confidence.*

4 Conclusion

Moving the sea ice framework in the IFS from an observation-space to a model-space control vector yields an overall neutral impact in terms of forecast quality, but with some evidence of forecast improvements, e.g. in the short range near the ice cap edges, and in some observational verification in the medium range Northern Hemisphere troposphere. These benefits arise despite both approaches producing similar sea ice concentration analyses. A key difference of the model-space method is that it allows the sea ice concentration analysis to be used as the background for the next assimilation cycle, resulting in a less biased first guess departure of the brightness temperatures for AMSR2 and, to a lesser extent, GMI, particularly during the simulated period of June–August 2022. This is also supported by the smaller average amplitude of sea ice concentration increments in the model-space approach compared to the observation-space approach. However, during December 2022–February 2023, the model-space approach shows a larger increase in the standard deviation of first guess departures for AMSR2 and GMI. Nevertheless, this increase does not appear to degrade the quality of the analysis.

The model-space approach presents several key advantages. First, by design, it does not require an instrument to have the 10 GHz channel as needed for the observation-space approach to construct the sea ice concentration background. For instance, the radiances of the Special Sensor Microwave Imager/Sounder (SSMIS) can be assimilated over sea ice. A preliminary study including SSMIS in this sea ice framework showed some significant differences around the polar ice caps with AMSR2 and GMI that will need to be addressed before including this instrument.

In upcoming IFS cycles, we plan to implement systematic re-screening for each outer loop of the 4DVar. This will allow new observations to enter the sea ice framework at any outer loop. In the observation-space approach, a first guess must be computed for each new observation set (using the 10 GHz channel). In contrast, the model-space approach allows these new observations to benefit from the sea ice concentration first guess field already optimized by the previous outer loop. This is potentially another key advantage of the model-space method for future IFS cycles.

Another benefit of the model-space approach is its ability to incorporate empirical state variables. While this requires assuming time-invariance of the empirical states within the assimilation window, a stronger constraint than that applied to sea ice concentration due to their expected temporal variability, it enables the cycling of these variables. The empirical states analysis can serve as the empirical states background for the next assimilation cycle. Preliminary experiments using this setup have shown promising results.

The next IFS cycle (CY50r1) will also have an outer loop coupling with the ocean. In this cycle, sea ice concentration estimated by the observation-space method (our Control approach) will be assimilated at AMSR2 observation locations in the ocean analyses. In return, the updated sea ice from the ocean analysis is used in subsequent coupled trajectories for data assimilation and in the longer range forecast. The model-space approach could also be used in the new outer loop coupling framework, simply by taking the XSIC analysis at AMSR2 and GMI observation locations. We will also investigate if the XSIC field could be integrated differently into the coupled system. A promising approach could be to use the SIC background from the ocean system (rather than cycling it through XSIC) while adding and cycling the empirical sea ice variables with the model-space approach.

Acknowledgements

The authors would like to thank Massimo Bonavita (ECMWF) for his comments and recommendations during the production of this document.

References

Bormann, N., Lawrence, H. and Farnan, J. (2019). Global observing system experiments in the ECMWF assimilation system. *ECMWF Technical Memoranda*, **Technical Memorandum No. 839**, doi:10.21957/sr184iyz, URL https://www.ecmwf.int/node/18859.

Eyre, J., Kelly, G., McNally, A. and Andersson, E. (1992). Assimilation of TOVS radiance information through one-dimensional variational analysis. *ECMWF Technical Memoranda*, **Technical Memorandum No. 187**, doi:10.21957/72yxf2jsk.

Fisher, M. and Andersson, E. (2001). Developments in 4D-Var and Kalman Filtering. *ECMWF Technical Memoranda*, **Technical Memorandum No. 347**.

Geer, A. J. (2024a). Joint estimation of sea ice and atmospheric state from microwave imagers in operational weather forecasting. *Quarterly Journal of the Royal Meteorological Society*, **150**(763), 3796–3826, URL https://doi.org/10.1002/qj.4797.

Geer, A. J. (2024b). Simultaneous inference of sea ice state and surface emissivity model using machine learning and data assimilation. *Journal of Advances in Modeling Earth Systems*, **16**(7), e2023MS004080, URL https://doi.org/10.1029/2023MS004080.

Le Dimet, F.-X. and Talagrand, O. (1986). Variational algorithms for analysis and assimilation of meteorological observations: theoretical aspects. *Tellus A*, **38A**(2), 97–110, doi:https://doi.org/10.1111/j.1600-0870.1986.tb00459.x, URL https://onlinelibrary.wiley.com/doi/abs/10.1111/j.1600-0870.1986.tb00459.x.

Massart, S., Bormann, N., Bonavita, M. and Lupu, C. (2021). Multi-sensor analyses of the skin temperature for the assimilation of satellite radiances in the European Centre for Medium-Range Weather Forecasts (ECMWF) Integrated Forecasting System (IFS, cycle 47R1). *Geosci. Model Dev.*, **14**(9), 5467–5485, doi:10.5194/gmd-14-5467-2021.

Zuo, H., Balmaseda, M. A., Tietsche, S., Mogensen, K. and Mayer, M. (2019). The ECMWF operational ensemble reanalysis–analysis system for ocean and sea ice: a description of the system and assessment. *Ocean Science*, **15**(3), 779–808, doi:10.5194/os-15-779-2019, URL https://os.copernicus.org/articles/15/779/2019/.

Appendix A XSIC vs CTR analyses of SIC and empirical variables

Appendix B Summary of the differences of sea ice and empirical states analyses

Table B.1: Summary of the mean difference and its standard deviation between the analysed values of the extended variables from model-space and observation-space approaches, computed from all GMI or AMSR2 observations using the sea ice framework, when the sea ice concentration analysis is greater than 10^{-2}. SIC: sea ice concentration, EP1 to EP3: empirical state variables.

			Global	S. Hemis.	N. Hemis.
SIC	JJA	GMI	-0.011 ± 0.053	-0.011 ± 0.052	-0.020 ± 0.078
	JJA	AMSR2	0.016 ± 0.044	0.010 ± 0.043	0.023 ± 0.045
	DJF	GMI	-0.013 ± 0.066	-0.010 ± 0.081	-0.016 ± 0.052
	DJF	AMSR2	-0.011 ± 0.042	-0.010 ± 0.069	-0.012 ± 0.031
EP 1	JJA	GMI	0.004 ± 0.017	0.004 ± 0.017	0.007 ± 0.024
	JJA	AMSR2	0.002 ± 0.017	0.001 ± 0.017	0.003 ± 0.016
	DJF	GMI	0.004 ± 0.023	-0.001 ± 0.027	0.009 ± 0.020
	DJF	AMSR2	0.000 ± 0.018	0.001 ± 0.027	0.000 ± 0.014
EP 2	JJA	GMI	0.005 ± 0.044	0.005 ± 0.044	-0.003 ± 0.040
	JJA	AMSR2	-0.000 ± 0.029	-0.002 ± 0.031	0.002 ± 0.026
	DJF	GMI	0.007 ± 0.048	-0.002 ± 0.046	0.015 ± 0.048
	DJF	AMSR2	-0.001 ± 0.031	-0.002 ± 0.041	-0.001 ± 0.029
EP 3	JJA	GMI	-0.003 ± 0.078	-0.003 ± 0.078	0.005 ± 0.086
	JJA	AMSR2	0.001 ± 0.065	0.003 ± 0.067	-0.003 ± 0.062
	DJF	GMI	-0.006 ± 0.085	-0.005 ± 0.088	-0.007 ± 0.082
	DJF	AMSR2	0.000 ± 0.067	-0.004 ± 0.094	0.001 ± 0.059

Table B.2: Number of observations used to compute the statistics of Tab. B.1

		Global	S. Hemis.	N. Hemis.
JJA	GMI	941,252	922,303	18,949
	AMSR2	2,932,697	1,691,795	1,240,902
DJF	GMI	350,607	150,759	199,848
	AMSR2	2,444,646	472,340	1,972,306

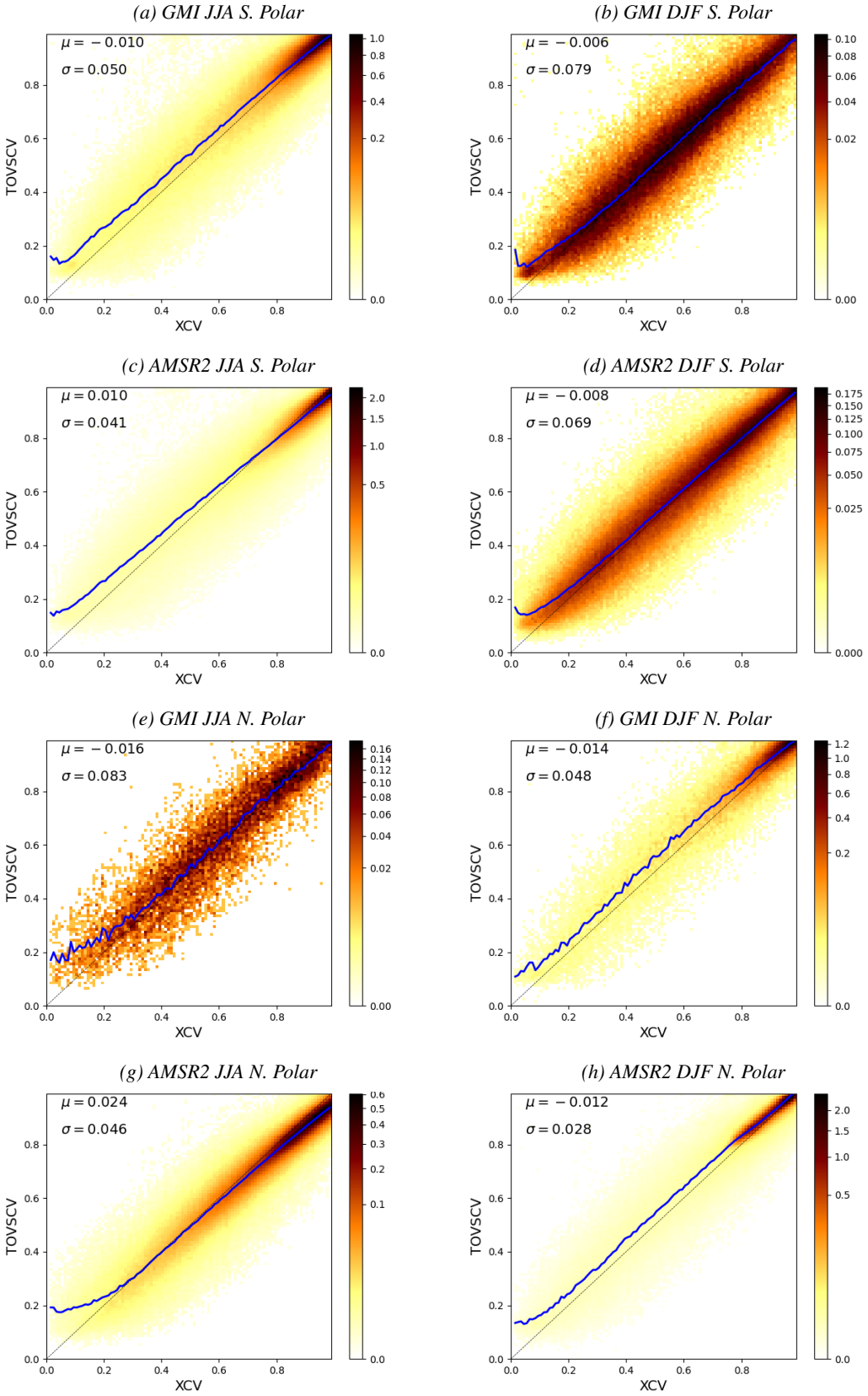

Figure A.1: Sea ice concentration value from TOVSCV versus XCV for the southern and northern polar regions, for the JJA and DJF seasons, and for GMI and AMSR2. The color represents the density of points and the blue line the mean value per bin; μ and σ are respectively the mean and standard deviation for the region and instrument.

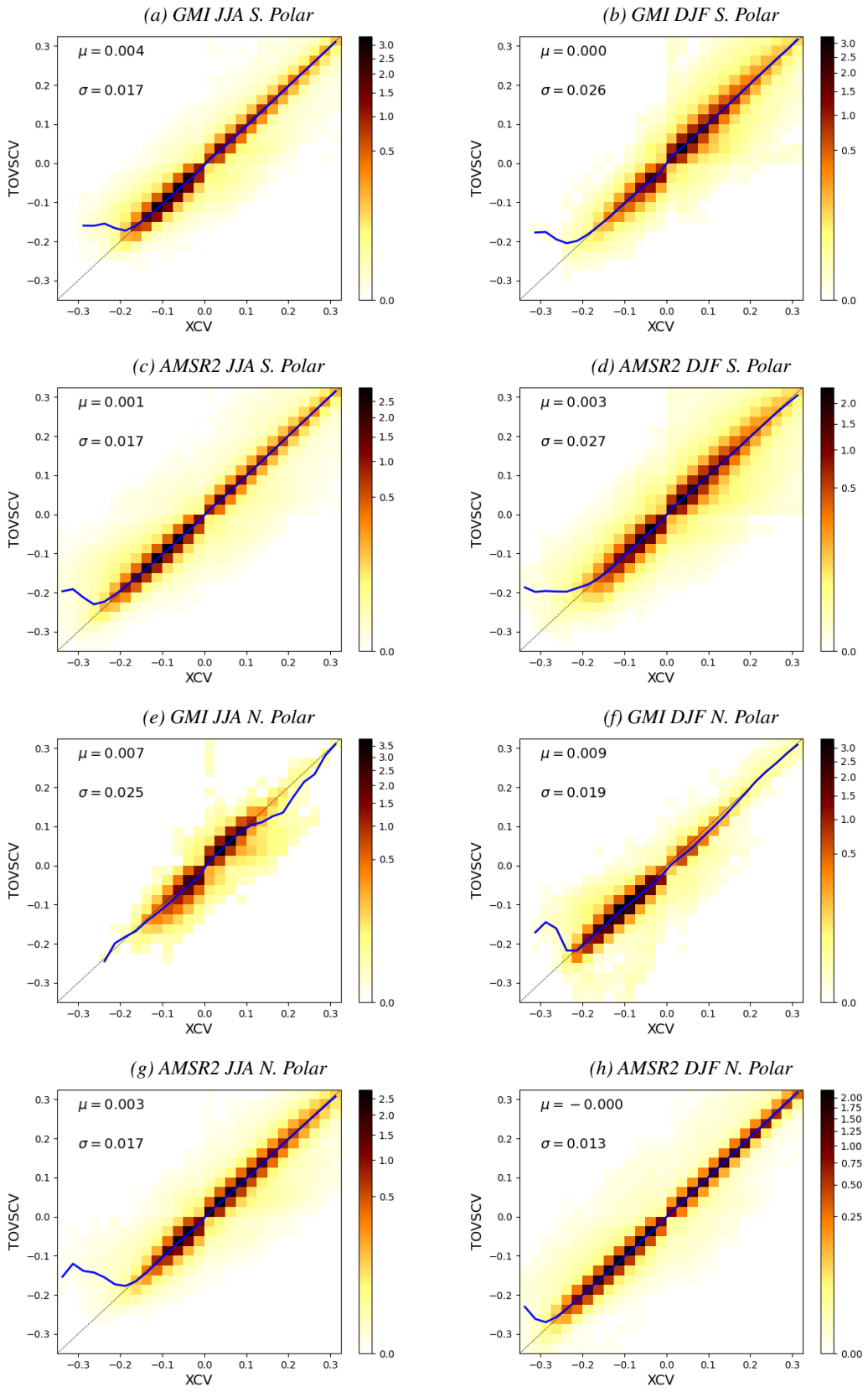

Figure A.2: Same as Fig. A.1 but for the empirical variable 1.

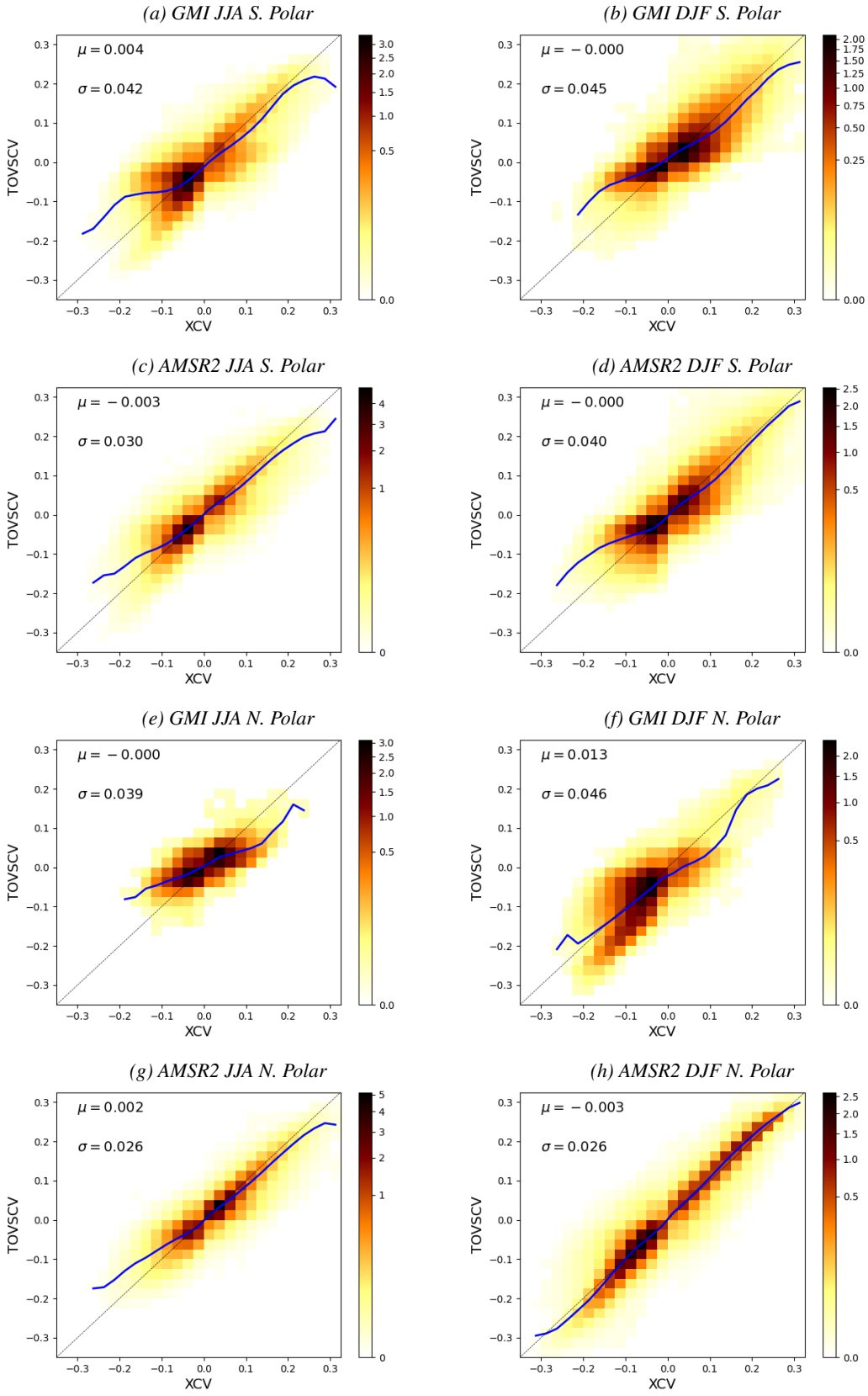

Figure A.3: Same as Fig. A.1 but for the empirical variable 2.

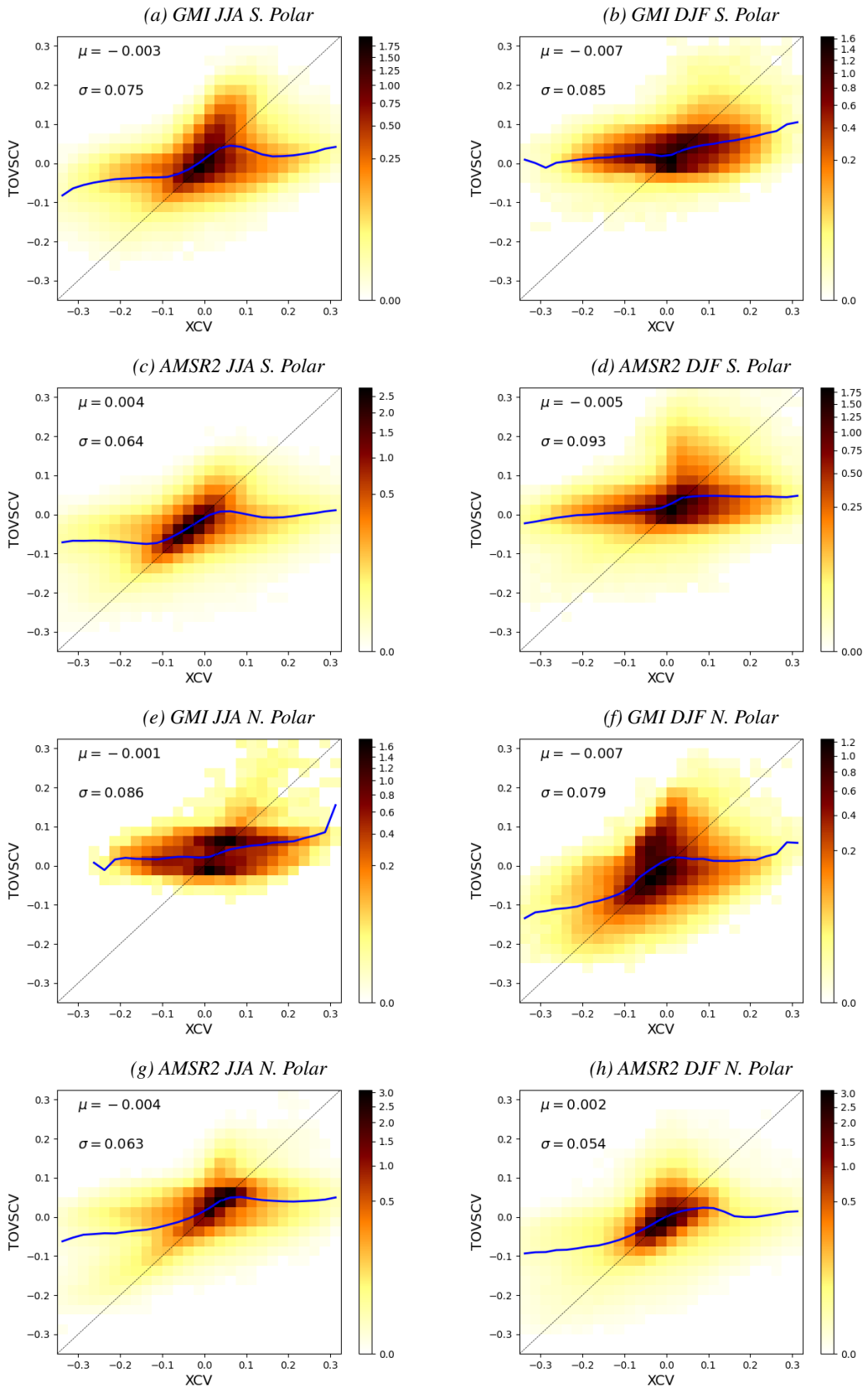

Figure A.4: Same as Fig. A.1 but for the empirical variable 3.

Appendix C Snapshot on 15 July 2022 00Z

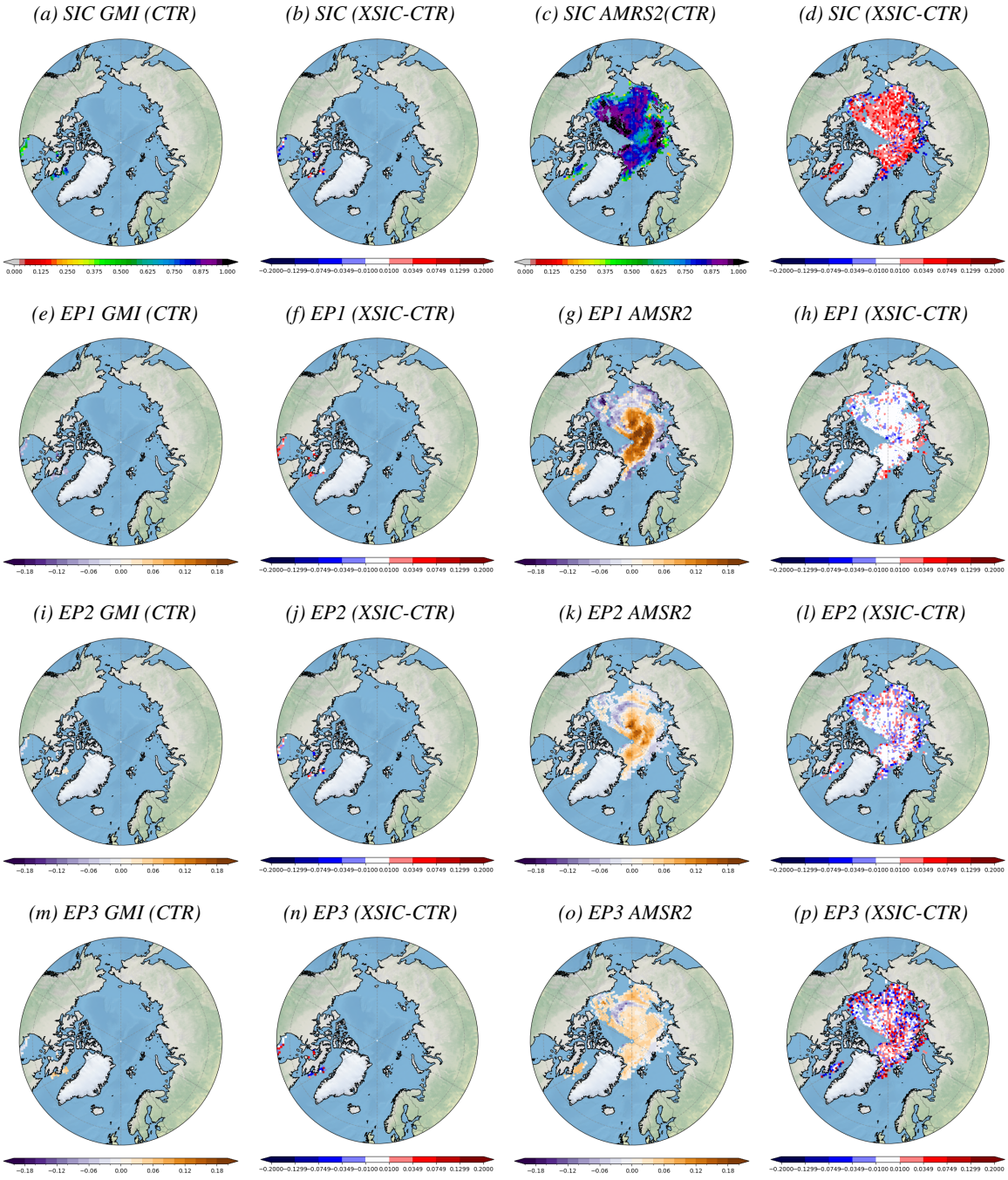

Figure C.5: SIC (top row) and empirical states (following rows) analyses from the control, for GMI (first column) and AMSR2 (third column) and difference between the XISC and control experiments (second and fourth column) for 15 July 2022.

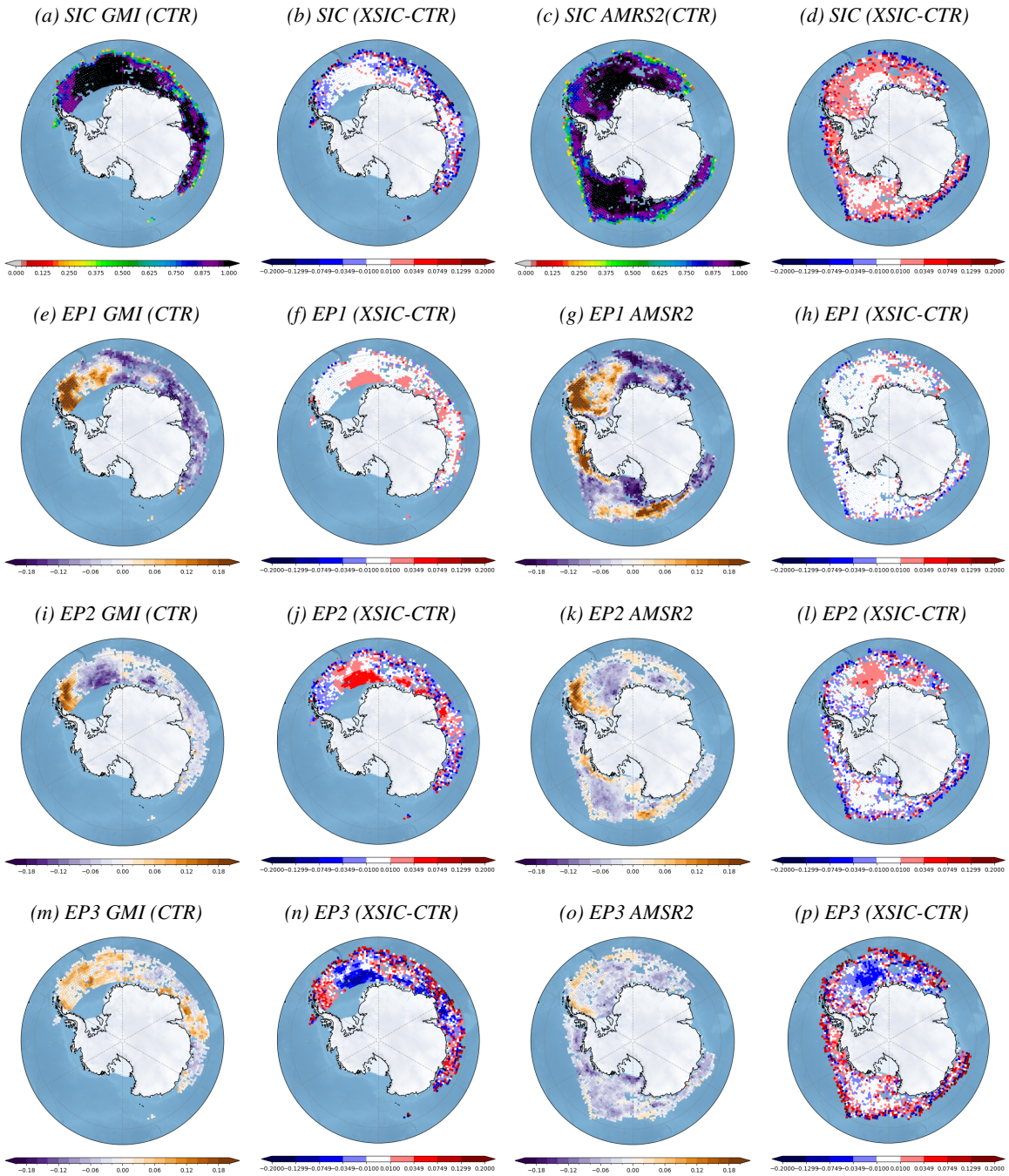

Figure C.6: Same as Fig. C.6 but for the Southern Hemisphere